Preparation and Characterization of Ferulic Acid-Wheat Gluten Nanofiber Films with Excellent Antimicrobial Properties

Chengming Jin , Huijuan Zhang , Feiyue Ren , Jing Wang , Sheng Yin *

Posted Date: 4 July 2023

doi: 10.20944/preprints202307.0168.v1

Keywords: wheat gluten (WG); ferulic acid; electrospinning; antimicrobial

Article

Preparation and Characterization of Ferulic Acid-Wheat Gluten Nanofiber Films with Excellent Antimicrobial Properties

Chengming Jin [1], Huijuan Zhang [1], Feiyue Ren [1], Jing Wang [1] and Sheng Yin [1,*]

[1] School of Food and Health, Beijing Technology & Business University (BTBU), Beijing 100048, China
China-Canada Joint Lab of Food Nutrition and Health (Beijing), Key Laboratory of Special Food Supervision Technology for State Market Regulation
* Correspondence: yinsheng@btbu.edu.cn

Abstract: In this study, composite nanofiber films comprising polyvinyl alcohol, wheat gluten, and glucose (PWG) were fabricated using electrospinning, followed by cross-linking via the Maillard crosslinking. Various mass concentrations of ferulic acid (FA) were incorporated into the PWG films. The results indicate that the average diameter of the FA-PWG films decreased from 449 nm to 331 nm as the concentration of FA increased, until reaching a concentration of 12%, after which a significant increase in diameter was observed. Subsequent Fourier transform infrared spectroscopy (FTIR), X-ray diffraction (XRD) and differential scanning calorimetry (DSC) results suggested that FA was distributed in the sample films in an amorphous form through hydrogen and ester bonds. Additionally, release experiments and antimicrobial tests on FA-PWG sample films showed good controlled release of FA and excellent anti-*Escherichia coli* and *Staphylococcus aureus* activity of this film. These findings all indicate that the FA-PWG nanofiber film is a potential candidate for food active packaging.

Keywords: wheat gluten (WG); ferulic acid; electrospinning; antimicrobial

1. Introduction

In recent times, electrospinning nanofiber films have gained widespread application in various fields, including bioscaffolds [1], drug delivery [2], and notably, active food packaging [3–5]. Active food packaging involves the integration of active molecules into packaging materials, leveraging the physicochemical properties of such molecules to safeguard foods [6]. The pivotal aspect of this process is the loading and subsequent release of the active molecules. Electrospinning offers distinct advantages, such as the ability to manipulate fiber morphology, achieve specific porosity, and attain a high volume to surface area ratio, rendering it an ideal technique for active packaging material preparation [7–9].

Materials used for food active packaging must be biodegradable polymers such as zein protein [10], chitosan [11], soy protein isolate [12], polyvinyl alcohol (PVA) [13], wheat gluten (WG) [4,14,15]. Of these options, WG has garnered significant attention due to its exceptional water stability and unique viscoelasticity [16]. In addition, WG exhibits outstanding film-forming properties, and its molecular structure contains numerous inter/intra-chain disulfide and hydrogen bonds, rendering it a superior raw material for electrospinning [17]. PVA is frequently utilized as a fundamental component for electrospinning blends, owing to its favorable biocompatibility and full biodegradability [18]. Previous studies have proved that both are suitable raw materials for loading active molecules. For instance, Aziz et al. [19] developed PVA/WG nanofiber film that was loaded with azathioprine, and the in vitro release outcomes indicated a reduction in the release of azathioprine following an initial sudden release, which was beneficial to the drug's therapeutic efficacy.

Nevertheless, the deficiencies in thermal stability and mechanical properties of PVA/WG nanofiber films limit their further applications [15]. Therefore, we considered the use of the Maillard cross-linking reaction to overcome these deficiencies. It has been demonstrated that this reaction can

 doi:10.20944/preprints202307.0168.v1

enhance the mechanical property and thermal stability of sample films. Zhang et al. [4] prepared a WG/zein composite nanofiber film, and found that the tensile strength was remarkable raised from 2.2 MPa to 9.5 MPa after xylose saccharification, and the denaturation temperature of the sample film rose to 135.8°C.

Ferulic acid (FA), also named as 3-methoxy-4-hydroxycinnamic acid, is a polyphenol derivative that possesses antioxidant properties. This phenolic acid is widely distributed in fruits, wholegrains, and plant cell walls, and is one of the effective constituents in several Chinese herbs, including Chuanxiong rhizome and Angelica sinensis [20]. It has obvious biological effects such as antioxidant, free radical scavenging, anti-infection and neuroprotection [13]. However, the poor water solubility and slow membrane absorption of FA significantly limit its utilization in active food packaging field [21]. Interestingly, these deficiencies can be override by blending electrospinning with the appropriate polymer matrix.

Therefore, we loaded FA into PVA/WG/glucose (PWG) nanofiber films cross-linked by Maillard to achieve sustainable release of FA while increasing the FA dissolution rate. The spinning solution was formulated by introducing varying concentrations of FA to the PWG mixed solution, followed by a comprehensive analysis of its physicochemical properties. The FA-PWG nanofiber films obtained after blending electrospinning were then heat-treated to achieve the Maillard cross-linking reaction. For the prepared sample films, a number of characterization analyses such as scanning electronic microscopy (SEM), Fourier transform infrared (FTIR), X-ray diffraction (XRD) and differential scanning calorimetry (DSC) were performed. Then, the release characteristics of FA-PWG films were studied using deionized water to simulate a high-moisture food matrix. Finally, typical food-borne pathogenic bacteria *Staphylococcus aureus* (*S. aureus*) and *Escherichia coli* (*E. coli*) were selected to verify the antimicrobial properties of the FA-PWG nanofiber films.

2. Materials and Methods

2.1. Materials

PVA (1788; Mw 19.8–26.4 kDa) with a degree of alcoholysis of 87.0%–89.0% (mol/mol) was obtained from MREDA Technology Co., Ltd. WG with an Mw of 30–90 kDa (model TII) was provided by Tokyo Chemical Industry Co., Ltd. Glucose (donated by Tianjin GreenBio Materials Co., Ltd) was used as a crosslinker for the Maillard reaction. *S. aureus* (CMCC26003) and *E. coli* (ATCC8099) were obtained from Beijing Sanyao Science & Technology and Nanjing Lezhen Biotechnology Co., Ltd.

2.2. Blending electrospinning

Dissolve 27% (w/v) of PVA/WG polymer in 50% acetic acid solution, with a mass ratio of 1:4. Then, glucose based on 20% of the mass of WG was added to the mixture to prepare a PWG solution. Subsequently, different masses of FA powders were added to the PWG solution to prepare FA-PWG mixed electrospinning solutions (FA levels: 0, 2, 4, 6, 8, 10, and 12 wt%, all weight based on WG), which were denoted FA0, FA2, FA4, FA6, FA8, FA10, and FA12, respectively.

All samples were loaded into medical syringes (5 mL) with 22G blunt needles and pumped through a syringe pump (Model HSP-101, MECC Co., Ltd., Japan) with the flow rate of 1.0 mL/h. Electrospinning voltage (Spellman High Voltage, Japan) and collector to syringe tip distance and were 25 kV and 10 cm. The FA-PWG nanofiber films obtained by electrospinning were collected on grounded square aluminum plates (15 x 15 cm) and then dried for 1 day at 25°C. The entire process of electrospinning was controlled at 45% relative humidity and 25°C. The resulting FA-PWG nanofiber films were thermally cross-linked at 150°C for 3 h.

2.3. Physicochemical properties of electrospinning solution

All samples were stirred overnight at 25 °C and then their surface tension, viscosity and conductivity were measured. The conductivity was measured by Malvern zeta potentiometer (ZS90, Malvern, Britain). The shear viscosity at shear rate 100 s^{-1} of electrospinning solutions were determined by TA rheometer (Discovery HR10, TA Instruments, US) with the parallel-plate of 50 mm

 doi:10.20944/preprints202307.0168.v1

diameter. The interface tensiometer (Theta Flex, Biolin Scientific AB, Sweden) was applied to measure surface tension of FA-PWG nanofiber films.

2.4. Morphology

The microscopic surface morphology of each sample films were investigated by SEM (S-4800, HITACHI, Japan). Among them, diameter distribution and average diameter of sample film was measured by the measurement of 50 fibers in 3 randomly elected SEM pictures using ImageJ software.

2.5. Compatibility of components

Infrared spectra of all sample films were measured with the Nicolet IS10 instrument (Thermo Fisher scientific, USA). The wavenumber range, resolution, and scans times of FTIR were 400-4000 cm^{-1}, 4 cm^{-1}, and 32, respectively.

2.6. Physical form

The XRD curve of the sample film was determined by D8 Advance diffractometer (Bruker AXS, Germany). The operating inclination, tube current, and tube voltage of the CuK α radiation source are 0.02°, 40 mA, and 40 kV, respectively. The measured wide angle diffraction range is 5° to 60° (2θ).

DSC curves of sample films were measured using DSC8000 equipment (PerkinElmer, US). Sample film (about 5 mg) was sealed in the aluminum crucible (40 μL). The films were heated from 30°C to 300°C with nitrogen atmosphere (0.05 L/min) at a heating rate of 10°C/min.

2.7. Active molecules release

The release behavior of FA-PWG nanofiber films in deionized water over 1440 min was investigated by modifying the methods reported by Huang et al. [21]. The FA-PWG nanofiber film was weighed 25 mg (±0.1 mg) each, placed in a beaker containing ultrapure water (50 mL), and stirred at 37°C in a water bath with a magnetic stirrer (100rpm). At specified time intervals (every 10 min for the first 60 min and every 60 min thereafter), supernatant (5 mL) was removed from the beaker and fresh ultrapure water (5 mL) was added. The absorbance value of the supernatant was measured by UV/vis spectrophotometer (Agilent Technologies Cary 100, USA) at 321 nm. The measured absorbances were brought to the pre-determined standard curve: $Y=0.0061X+0.011$ ($R^2=0.9986$), where X value is the concentration of FA (μg/mL), and Y value was the absorbance at 321 nm. And calculate the cumulative release of FA at that moment according to Equation (1):

$$\text{Accumulative release (\%)}=\frac{W_t}{W_d}\times 100\% \qquad (1)$$

where W_t is the release amount of FA in time t, and W_d is the whole loading amount of FA in nanofiber film.

The spreading, solubilizing and eroding mechanisms of active molecules are the most essential rate governing mechanisms for release control products [22]. For better representation the release mechanism of FA from PWG sample films, four release kinetic models including First-order (Equation (2)), Zero-order (Equation (3)), Korsmeyer-Peppas (Equation (4)), and Higuchi (Equation (5)) were used to study the FA-PWG nanofiber films [23–26].

$$\ln(1-M_t/M_\infty)=-k_F t \qquad (2)$$

$$M_t/M_\infty=k_Z t \qquad (3)$$

$$M_t/M_\infty=k_K t^n \qquad (4)$$

$$M_t/M_\infty=k_H t^{0.5} \qquad (5)$$

M_t/M_∞ are the release ratios of FA molecules at moments t, K_F, K_Z, K_K and K_H are the constant parameters of First-order, Zero-order, Korsmeyer-Peppas and Higuchi equations, respectively, and n is diffusion index.

Preprints (www.preprints.org) | NOT PEER-REVIEWED | Posted: 4 July 2023 doi:10.20944/preprints202307.0168.v1

2.8. Antimicrobial test

The plate agar disc diffusion methods were applied to evaluate the antimicrobial performance of FA-PWG sample films. After culturing *S. aureus* and *E. coli* to fourth generation strains, gradient dilutions (~10^6 CFU/mL) were performed. Dilution (about 100 μL) was taken for plate coating, and a triangular glass rod was used to disperse the bacterial solution evenly. The sample film electrospun on aluminum foil was cut into 6 mm discs and disinfected using UV for 1 h. Then, the FA-PWG nanofiber films were placed in a coated plate and incubated at 37 °C for 24 h in a constant temperature incubator to measure the inhibition zone diameter.

2.9. Statistical analysis

Statistical analysis was performed by IMB SPSS Statistics 26 software and results was reported as mean ± standard deviation (SD). One-way analysis of variance (ANOVA) and Duncan analysis were used for data analysis. Significant difference was considered at $P < 0.05$. All experiments were performed in triplicate.

3. Results and discussion

3.1. Solution properties

The success of electrospinning is contingent upon the physicochemical property of electrospinning solution, specifically its surface tension, viscosity, and conductivity [7]. Table 1 shows the physicochemical property of PWG electrospinning solutions with different concentrations of FA. It was not difficult to see that with the augmentation of FA mass concentration in the mixed solvent, the surface tension and viscosity of FA-PWG spinning solution boosted. Additionally, the conductivity reaches the maximum at FA10, which is 1.28 ms/cm. There were no significant differences in the physicochemical property between FA0 and FA2 electrospinning solutions ($p>0.05$). With the increasing addition (from FA0-FA12), the viscosity increased continuously from 2.01 to 2.45 Pa.s. The increase in solution viscosity can be explained by the formation of molecular clusters between PVA/WG/G-FA, which increases the degree of entanglement between polymer molecular chains in solution, thereby enhancing the electrospinning ability of the solution [27]. However, the conductivity in the FA-PWG solution showed a downward trend in the FA12 solution.

Excessive solution viscosity or inadequate conductivity will hinder the stretching of the fiber during electrospinning, making the resulting nanofibers thicker [16]. Within a specific range, higher solution conductivity facilitates greater fiber stretching and differentiation, resulting in smaller fiber diameters. Niloufar et al. [28] prepared FA-cyclodextrin inclusion complex nanofiber pad and found that the conductivity of the sample increased at first and then decreased, with the increasing FA concentration, which was consistent with the results of this experiment.

Table 1. Characterization of physicochemical properties of PVA/WG/G electrospinning solution with different concentrations of FA.

Sample (FA-PWG)	Conductivity (ms/cm)	Viscosity (Pa.s)	Surface Tension (mN/m)
FA0	1.03 ± 0.05^{e}	2.01 ± 0.08^{e}	29.81 ± 0.13^{d}
FA2	1.06 ± 0.04^{de}	2.06 ± 0.02^{e}	29.92 ± 0.48^{cd}
FA4	1.15 ± 0.02^{bc}	2.15 ± 0.05^{d}	30.96 ± 0.71^{cd}
FA6	1.18 ± 0.02^{bc}	2.18 ± 0.02^{cd}	31.26 ± 0.95^{bcd}
FA8	1.23 ± 0.04^{ab}	2.26 ± 0.03^{c}	31.57 ± 0.28^{bc}
FA10	1.28 ± 0.02^{a}	2.36 ± 0.04^{b}	32.48 ± 0.47^{b}
FA12	1.12 ± 0.07^{cd}	2.45 ± 0.05^{a}	34.19 ± 0.96^{a}

All values are mean ± standard deviation of three replicates. Different lowercase letters in the same column indicate significant difference ($p<0.05$). FA: ferulic acid; PVA: polyvinyl alcohol; WG: wheat gluten; G: glucose.

Preprints (www.preprints.org) | NOT PEER-REVIEWED | Posted: 4 July 2023 doi:10.20944/preprints202307.0168.v1

3.2. Morphology

An analysis of the SEM images reveals that the average diameter of FA-PWG nanofiber films exhibits a trend of initially decreasing and subsequently increasing with an increase in FA loading concentration (Figure 1). Notably, the FA-PWG nanofiber films exhibit relatively smooth surfaces, and the absence of granular substances on the fiber surface suggests that FA has been uniformly dispersed in the PWG matrix. The average diameter of nanofiber film FA0 is 449 nm, when the addition of FA is 10%, the diameter of nanofiber film FA10 is the smallest, which is 331 nm. However, when the addition of FA reached 12%, the average diameter of the nanofiber film FA12 boosted to 509 nm. These findings align with Asli et al.'s research, which similarly found that pure hydroxypropyl-γ-cyclodextrin nanofibers had a greater average diameter than FA/cyclodextrin inclusion complex [29]. This disparity was owing to the higher conductivity and lower solution viscosity than hydroxypropyl-γ-cyclodextrin solution of FA/cyclodextrin inclusion complexes solution. As we all know, the decrease of fiber diameter is not only conducive to the full cross-linking reaction, so that the non-protonated amino and electrophilic carbonyl groups can be fully exposed, but also improve the loading of nanofiber films to active molecules [30]. Deng et al. [31] prepared gelatin/zein nanofiber films loaded with allopurinol, and observed that the composite nanofibers loaded with 2.5% allopurinol had the smallest average diameter and the highest entrapment efficiency, which were 244.1 nm and 94.92%.

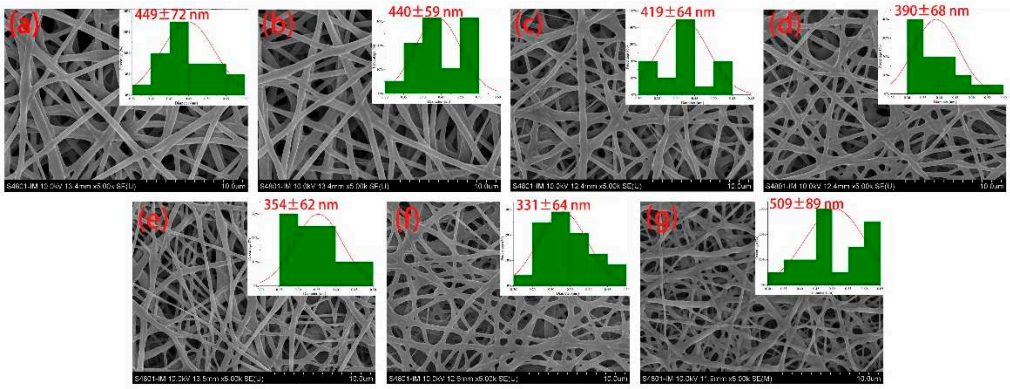

Figure 1. SEM images of PVA/WG/G composite nanofiber films loaded with different concentrations of FA: (**a**) FA0; (**b**) FA2; (**c**) FA4; (**d**) FA6; (**e**) FA8; (**f**) FA10; (**g**) FA12. Data are presented as mean values ± standard deviation.

3.3. Component interaction analysis

FTIR spectra of FA and FA-PWG nanofiber films are presented in Figure 2A. The characteristic peaks of FA at 1687 cm^{-1} and 1660 cm^{-1} are formed by the stretching vibration of C=O, which indicates that the presence of carbonyl groups in the crystal lattice of FA [21]. The characteristic absorption peak at 3435 cm^{-1} is related to the O-H stretching vibration. Additionally, the characteristic absorption peaks of FA at 2969 cm^{-1} and 1265 cm^{-1} are related to the C-H stretching vibration and the C-O-C asymmetric stretching vibration [32]. The characteristic absorption peak at 1376 cm^{-1} is related to the aromatic nucleus in FA molecule, and the characteristic absorption peaks at 850 cm^{-1} and 801cm^{-1} are caused by two adjacent H atoms on the benzene ring of the FA molecule [33]. These chemical bonds in different vibrational forms reflect the ordered crystal structure of FA molecules. However, for the nanofiber film FA-PWG, the characteristic peak of FA in the infrared spectrum disappears, indicating that FA in the nanofiber film does not form the FA dimer necessary for lattice construction [21,34].

Firstly, with the increasing FA addition, O-H stretching vibration peak in FA-PWG nanofiber films shifted from 3281 (FA0) to 3285 (FA6) and 3290 cm^{-1} (FA10). Secondly, the stretching vibration peak of WG amide I band in FA-PWG nanofiber films shifted from 1639 (FA0) to 1644 (FA2) and 1655 cm^{-1} (FA12) higher wavenumber. These phenomenon are due to the chemical interaction between FA and the components of the FA-PWG film, and it is speculated that this interaction is hydrogen bond (Figure 2B) [13,29,35]. Finally, the addition of FA also led to a weakening of the N-H bending

Preprints (www.preprints.org) | NOT PEER-REVIEWED | Posted: 4 July 2023 doi:10.20944/preprints202307.0168.v1

vibrations associated with amide II band, which may be related to the presence of esterification reactions between some of the amino acids in WG (e.g., Ser and Tyr) and FA [3].

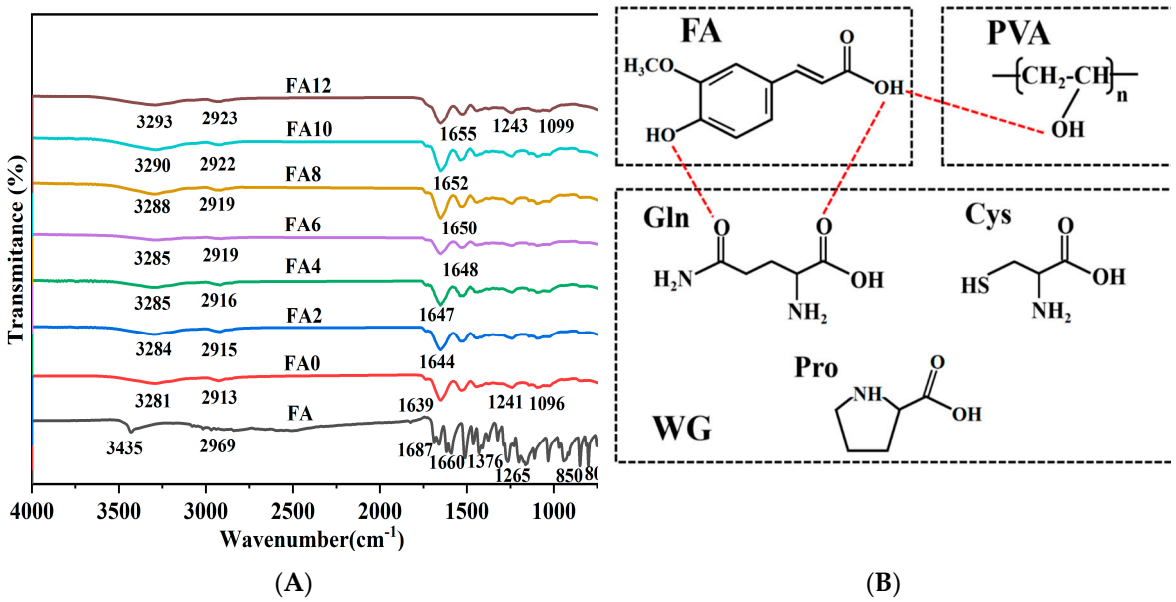

Figure 2. (A) FTIR spectra of FA powder and PVA/WG/G composite nanofiber films loaded with different concentrations of FA, **(B)** The molecular formula of FA, PVA and WG.

3.4. Physical state analysis

The utilization of X-ray diffraction (XRD) analysis is a common practice in the characterization of the crystalline state of a substance. The amorphous dispersion of active molecules in nanofibers is generally regarded as advantageous for their dissolution and release [36]. As depicted in Figure 3A, the XRD images of FA and FA-PWG nanofiber films. It can be clearly observed that the FA has many diffraction peaks of different intensities, indicating that it is a crystalline substance [37]. The diffraction pattern of FA-PWG nanofiber films exhibits a resemblance to that FA0. The absence of characteristic diffraction peak associated with the crystalline phase of FA suggests the existence of amorphous FA in FA-PWG nanofiber film. This may be connected with the chemical interaction between FA and WG during the process of electrospinning. It is widely acknowledged that the quick evaporation of solvent during electrospinning hinders the crystallization of active molecules [38]. In contrast, the FA/hydroxypropyl-β-cyclodextrin composite nanofiber films prepared by Asli et al. [29] still contained some uncomplexed FA crystals. The amorphous distribution of FA in the composite nanofiber films is consistent with the notion of loading active molecules in functional fibers food packaging and the controllable release characteristics of active molecules [21]. Therefore, the FA-PWG nanofiber films prepared in this study are suitable for active packaging materials.

Figure 3B shows the DSC results of FA and FA-PWG nanofiber film, and the results are in full agreement with those of XRD. FA has a sharp thermal absorption peak at 174.38 ℃, indicating its crystal state. Nonetheless, the FA-PWG nanofiber films did not exhibit the thermal absorption peak of FA, which indicates that the active molecule was present in an amorphous state within the fibers. The shape of the DSC curve of the FA-PWG nanofiber films loaded with FA, although consistent with that of FA0, corresponds to a different value of enthalpy change. This may be related to the chemical interaction (hydrogen bond formation) between the active molecule FA and the components of composite nanofiber films [39].

Preprints (www.preprints.org) | NOT PEER-REVIEWED | Posted: 4 July 2023 doi:10.20944/preprints202307.0168.v1

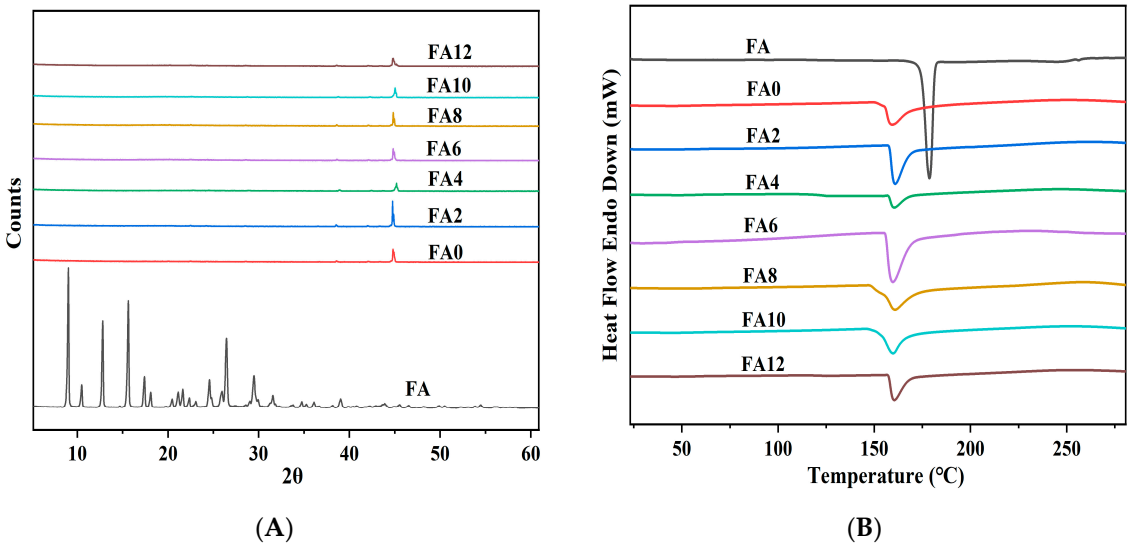

Figure 3. (A) XRD patterns and **(B)** DSC thermograms of FA powder and PVA/WG/G composite nanofibers loaded with different concentrations of FA.

3.5. Release performance

The release curve of FA-PWG nanofiber film was presented in Figure 4. In the initial 60 min, each FA-PWG nanofiber film showed a rapid release behavior, with a release rate of about 14%, which may be related to the dissolution of FA adhered to the fiber surface or embedded in a shallow position inside the fiber. In another study, the PVA nanofiber film loaded with γ-cyclodextrin/FA inclusion complex prepared by Vimalasruthi et al. [13] did not have fast release behavior, and the release rate of FA was less than 6% at 60 min. During 60–720 min, the release percentage of FA in the composite nanofibers increased slowly over time. After 720 min, the FA release rate tended to be stable, and the release percentage of FA10 was the highest, which was 97.38%. The aforementioned occurrence may be ascribed to the continuous relaxation and disintegration of the interior of the composite nanofibers under the attack of water molecules over time, thereby slowly exposing the FA located inside the fibers. Gyuldzhan et al. [40] prepared polycaprolactone/chitosan composite nanofiber films loaded with FA by electrospinning. Their in vitro release findings indicated that the highest rate of FA release was merely 91.4%, which was significantly lower than the rate observed in the current study.

For FA12, it has the lowest final release rate of only 93.24%, which may be related to the diameter distribution of composite nanofibers. The relationship between fiber diameter and specific surface area is widely acknowledged, as smaller diameters result in increased surface contact between active molecules and dissolution medium solutions, leading to higher release rates [41]. These FA-PWG nanofiber films with both initial blast release and later sustained release properties, exhibits significant possibilities for employment in active food packaging. It is well-suited for use in food packaging susceptible to rapid oxidation, as well as in packaging necessitating continuous and effective antioxidant properties [21].

As shown in Table 2, all model release kinetic parameters of samples were compared, and the Korsmeyer-Peppas model had a high coefficient of determination (R^2>0.95), suggesting that this model was more suitable for describing the release of FA in PWG composite nanofibers. In the Korsmeyer-Peppas model, when n ≤ 0.45 the corresponding release mechanism is the Fickian diffusion mechanism [42]. If the value of n falls between 0.45 and 0.89, the mechanism is non-Fickian, where the diffusion mechanism is mainly controlled by the combination of relaxation and diffusion of macromolecular chain segments [43]. When n=0.89, the kinetics is Zero-order release model, which is ideal, implying complete release of the encapsulated active molecules. When n>0.89, release mechanism is the super Case II release mechanism [44]. At this time, the release of the active molecule FA follows complexes release mechanism including diffusion, expansion, and erosion, in which the erosion of the carrier is the mainly dominant. Thus, the release of FA-PWG nanofiber films in

Preprints (www.preprints.org) | NOT PEER-REVIEWED | Posted: 4 July 2023 doi:10.20944/preprints202307.0168.v1

ultrapure water is a complex process, in which cross-linked relaxation and erosion of the negative carrier nanofiber films dominate (Figure 5).

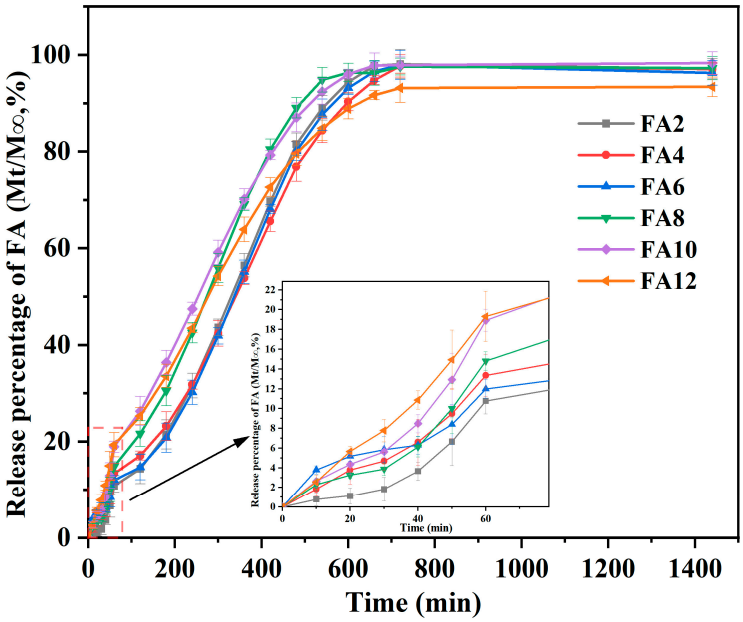

Figure 4. Release curves of FA-PWG composite nanofiber films loaded with different concentrations of FA.

Table 2. Kinetic parameters of FA release from the prepared composite nanofiber films.

Formulation	Zero-order		First-order		Higuchi		Korsmeyer-Peppas			Release rate (%)
	K_Z	R^2	K_F	R^2	K_H	R^2	K_K	n	R^2	
FA2	0.0904	0.6931	0.0034	0.7578	4.0457	0.8533	0.0501	1.1809	0.9844	97.15
FA4	0.0901	0.7499	0.0031	0.7962	3.7053	0.8884	0.3171	0.8696	0.9796	96.25
FA6	0.0906	0.7314	0.0032	0.7721	3.7247	0.8661	0.3823	0.8393	0.9664	96.17
FA8	0.0902	0.6986	0.0033	0.7623	3.8357	0.8853	0.2083	0.9697	0.9765	96.37
FA10	0.1186	0.5302	0.0034	0.8167	3.7368	0.9007	0.3263	0.9018	0.9686	97.38
FA12	0.0815	0.732	0.0025	0.8219	3.4398	0.9141	0.7767	0.7303	0.9737	93.24

All values are mean of three replicates. FA: ferulic acid.

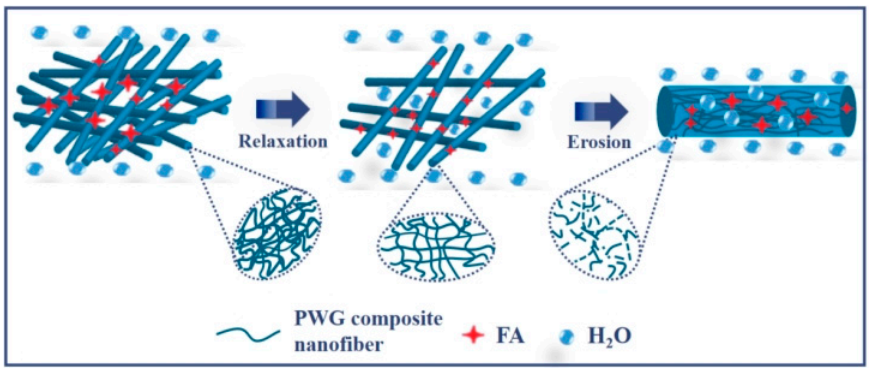

Figure 5. Schematic diagram of the release characterization of the active molecule FA.

3.6. Antibacterial property analysis

Figure 6 presents the diameter of the inhibitory zone of FA-PWG nanofiber films. It can be clearly seen that FA0 has no inhibition function on both *S. aureus* and *E. coli*, and the sample film with FA addition has better inhibition function on *S. aureus* than *E. coli*. The same phenomenon also appeared in a research of Jia et al [32]. With the increase of FA loading in the sample films, the diameter of the

Preprints (www.preprints.org) | NOT PEER-REVIEWED | Posted: 4 July 2023 doi:10.20944/preprints202307.0168.v1

inhibitory circle of FA-PWG nanofiber film enhanced continuously. At FA12, the diameter of the inhibitory zone of the sample film reached the maximum of 1.918 cm for *S. aureus* and 1.447 cm for *E. coli*. It was not difficult to find that the inhibition effect increased significantly ($p < 0.05$) at 2% to 10% of FA addition, while no obvious differences were observed when the FA level was 12%. The observed phenomenon can be ascribed to the augmentation in the diameter of the FA12 nanofiber film, which hinders the diffusion of active molecules and the diffusion resistance of the agar medium [15]. Currently, the bactericidal mechanism of FA is generally believed to be through modification of bacterial cell membranes, changing the hydrophobicity of cell membranes, resulting in localized rupture of bacterial cell membranes, thus providing bactericidal effects [32,40].

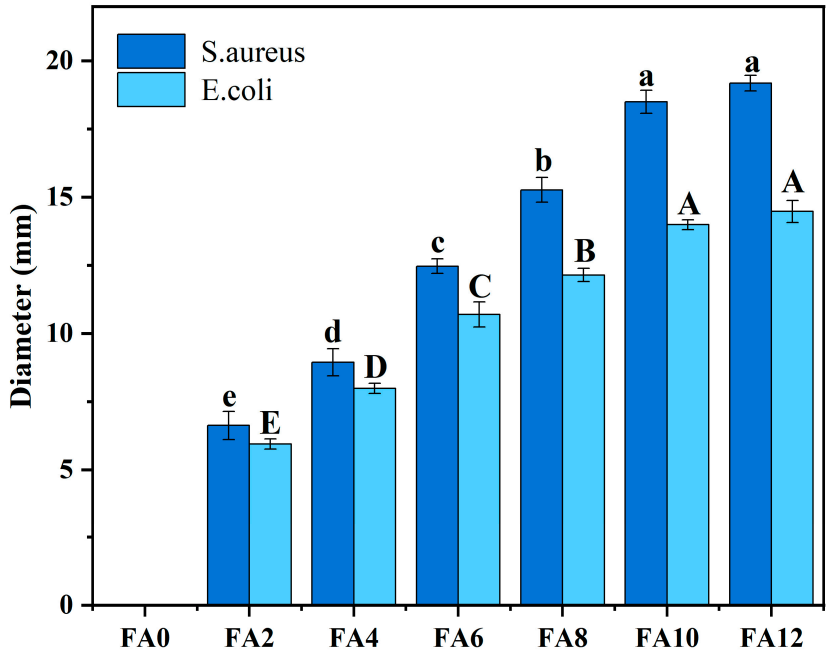

Figure 6. Diameter of inhibition zone of sample film. Different letters in the same set of charts indicate significant differences ($p<0.05$).

4. Conclusions

In this study, PWG nanofiber films loaded with active molecular FA were prepared by blending electrospinning. In the group of FA0-FA10, the diameter of the sample nanofiber film decreases continuously along with the increase of the solution conductivity. However, for FA12, the increase in solution viscosity and the decrease in conductivity led to an increase in nanofiber film diameter. The findings from FTIR, XRD and DSC analyses suggest that chemical interactions (e.g., esterification reactions and hydrogen bonding) exist between FA and various components of the FA-PWG film and are distributed in the film in an amorphous form. Subsequent release studies revealed that the Korsmeyer-Peppas model accurately reveals the release of FA in the PWG sample film, and the release process mostly consists of carrier swelling and erosion. Antibacterial tests showed that the sample films had excellent antibacterial properties and were better resistant to *S. aureus* than *E. coli.* Therefore, FA-PWG nanofiber films can be candidates for antimicrobial food packaging materials.

Author Contributions: C. J.: writing-review, editing, and conceptualization; H. Z.: funding acquisition, resources and reviewing; F. R.: supervision, formal analysis; J. W.: Funding acquisition, Resources; S. Y.: reviewing, supervision. All authors have read and agreed to the published version of the manuscript.

Funding: This work was supported by the Beijing Natural Science Foundation (No. 6232001); Cultivation Project of Double First-Class Disciplines of Food Science and Engineering, Beijing Technology & Business University (No. 19008022213); and Key R&D Program of Shandong Province (2021CXGC010807).

Data Availability Statement: All data is contained within the article.

Conflicts of Interest: The authors declare that there is no conflict of interest.

References

1. Peng; Wen; Yan; Wen; Min-Hua; Zong; Robert; J.; Linhard; Hong. Encapsulation of Bioactive Compound in Electrospun Fibers and Its Potential Application. Journal of Agricultural & Food Chemistry **2017**.
2. Kumar, C.S.; Soloman, A.M.; Thangam, R.; Perumal, R.K.; Gopinath, A.; Madhan, B. Ferulic acid-loaded collagen hydrolysate and polycaprolactone nanofibres for tissue engineering applications. Iet Nanobiotechnology **2020**, 14, 202-209, doi:10.1049/iet-nbt.2019.0281.
3. Li, T.; Xia, N.; Xu, L.N.; Zhang, H.; Zhang, H.J.; Chi, Y.J.; Zhang, Y.L.; Li, L.L.; Li, H.Y. Preparation, characterization and application of SPI-based blend film with antioxidant activity. Food Packaging and Shelf Life **2021**, 27, doi:10.1016/j.fpsl.2020.100614.
4. Zhang; Deng, L.L.; Zhong, H.; Zou, Y.C.; Qin, Z.Y.; Li, Y.; Zhang, H. Impact of glycation on physical properties of composite gluten/zein nanofibrous films fabricated by blending electrospinning. Food Chemistry **2022**, 366, doi:10.1016/j.foodchem.2021.130586.
5. Wang, P.; Li, Y.; Zhang, C.; Que, F.; Weiss, J.; Zhang, H. Characterization and antioxidant activity of trilayer gelatin/dextran-propyl gallate/gelatin films: Electrospinning versus solvent casting. Lwt-Food Science and Technology **2020**, 128, doi:10.1016/j.lwt.2020.109536.
6. Li, W.H.; Zhang, C.; Chi, H.; Li, L.; Lan, T.Q.; Han, P.; Chen, H.Y.; Qin, Y.Y. Development of Antimicrobial Packaging Film Made from Poly(Lactic Acid) Incorporating Titanium Dioxide and Silver Nanoparticles. Molecules **2017**, 22, doi:10.3390/molecules22071170.
7. Haider, A.; Haider, S.; Kang, I.K. A comprehensive review summarizing the effect of electrospinning parameters and potential applications of nanofibers in biomedical and biotechnology. Arabian Journal of Chemistry **2015**, 11, 1165-1188, doi:10.1016/j.arabjc.2015.11.015.
8. Xue; Tong; Wu; Yunqian; Dai; Younan; Xia. Electrospinning and Electrospun Nanofibers: Methods, Materials, and Applications. Chemical reviews **2019**, 119, 5298-5415, doi:10.1021/acs.chemrev.8b00593.
9. Cen, Z.; Yang, L.; Peng, W.; Hui, Z. Electrospinning of nanofibers: potentials and perspectives for active food packaging. Comprehensive Reviews in Food Science and Food Safety **2020**, 19, 479-502, doi:10.1111/1541-4337.12536.
10. Liu, F.G.; Li, X.Z.; Wang, L.; Yan, X.J.; Ma, D.X.; Liu, Z.G.; Liu, X.B. Sesamol incorporated cellulose acetate-zein composite nanofiber membrane: An efficient strategy to accelerate diabetic wound healing. International Journal of Biological Macromolecules **2020**, 149, 627-638, doi:10.1016/j.ijbiomac.2020.01.277.
11. Riaz, A.; Lagnika, C.; Luo, H.; Dai, Z.Q.; Nie, M.M.; Hashim, M.M.; Liu, C.Q.; Song, J.F.; Li, D.J. Chitosan-based biodegradable active food packaging film containing Chinese chive (Allium tuberosum) root extract for food application. International Journal of Biological Macromolecules **2020**, 150, 595-604, doi:10.1016/j.ijbiomac.2020.02.078.
12. Nassar, S.F.; Dombre, C.; Gastaldi, E.; Touchaleaume, F.; Chalier, P. Soy protein isolate nanocomposite film enriched with eugenol, an antimicrobial agent: Interactions and properties. Journal of Applied Polymer Science **2018**, 135, doi:10.1002/app.45941.
13. Vn, A.; Mkm, B.; St, A. Electrospinning preparation and spectral characterizations of the inclusion complex of ferulic acid and γ-cyclodextrin with encapsulation into polyvinyl alcohol electrospun nanofibers. Journal of Molecular Structure 2020, 1221.
14. Zhang; Deng, L.; Zhong, H.; Pan, J.; Zhang, H. Superior water stability and antimicrobial activity of electrospun gluten nanofibrous films incorporated with glycerol monolaurate. Food Hydrocolloids **2020**, 109, 106-116, doi:10.1016/j.foodhyd.2020.106116.
15. Wang; Yi, S.; Chu, C.; Liu, H.; Jiang, S. Preparation, antimicrobial and release behaviors of nisin-poly (vinyl alcohol)/wheat gluten/ZrO2 nanofibrous membranes. Journal of Materials Science **2015**, 50, 5068-5078, doi:10.1007/s10853-015-9059-0.
16. Zhang, H.J.; Jin, C.M.; Lv, S.H.; Ren, F.Y.; Wang, J. Study on electrospinning of wheat gluten: A review. Food research international **2023**, 169, 112851, doi:10.1016/j.foodres.2023.112851.
17. Han, Y.; Chen, H. Enhancement of nanofiber elasticity by using wheat glutenin as an addition. Polymer Science **2013**, 55, 320-326, doi:10.1134/S0965545X13050076.
18. Ugur, M.H.; Oktay, B.; Gungor, A.; Kayaman-Apohan, N. Highly thermally resistant, hydrophobic poly(vinyl alcohol)-silica hybrid nanofibers. Journal of the Serbian Chemical Society **2018**, 83, 885-897, doi:10.2298/jsc171121032h.
19. Aziz, S.; Hosseinzadeh, L.; Arkan, E.; Azandaryani, A.H. Preparation of electrospun nanofibers based on wheat gluten containing azathioprine for biomedical application. International Journal of Polymeric Materials **2019**, 68, 639-646, doi:10.1080/00914037.2018.1482464.
20. Zhao, Z.H.; Moghadasian, M.H. Chemistry, natural sources, dietary intake and pharmacokinetic properties of ferulic acid: A review. Food Chemistry **2008**, 109, 691-702, doi:10.1016/j.foodchem.2008.02.039.
21. Huang, X.Y.; Jiang, W.L.; Zhou, J.F.; Yu, D.G.; Liu, H. The Applications of Ferulic-Acid-Loaded Fibrous Films for Fruit Preservation. Polymers **2022**, 14, doi:10.3390/polym14224947.

22. Langer, R.; Peppas, N. Chemical and Physical Structure of Polymers as Carriers for Controlled Release of Bioactive Agents: A Review. Polymer Reviews **1983**, 23, 61-126.
23. Lobo, C. Modeling and comparison of dissolution profiles. European Journal of Pharmaceutical Sciences **2001**, 13, 123-133, doi:10.1016/S0928-0987(01)00095-1.
24. Neo, Y.P.; Swift, S.; Ray, S.; Gizdavic-Nikolaidis, M.; Jin, J.Y.; Perera, C.O. Evaluation of gallic acid loaded zein sub-micron electrospun fibre mats as novel active packaging materials. Food Chemistry **2013**, 141, 3192-3200, doi:10.1016/j.foodchem.2013.06.018.
25. Higuchi, T. Theoretical analysis of rate of release of solid drugs dispersed in solid matrices. Journal of pharmaceutical sciences **1963**, 52, 1145-1149, doi:10.1002/jps.2600521210.
26. Korsmeyer, R.W.; Gurny, R.; Doelker, E.; Buri, P.; Peppas, N.A. Mechanisms of Solute Release from Porous Hydrophilic Polymers. International Journal of Pharmaceutics **198**3, 15, 25-35, doi:10.1016/0378-5173(83)90064-9
27. Yang, J.L.; Yu, K.; Tsuji, T.; Jha, R.; Zuo, Y.Y. Determining the surface dilational rheology of surfactant and protein films with a droplet waveform generator. Journal of Colloid and Interface Science **2019**, 537, 547-553, doi:10.1016/j.jcis.2018.11.054.
28. Sharif, N.; Golmakani, M.T.; Niakousari, M.; Hosseini, S.M.H.; Ghorani, B.; Lopez-Rubio, A. Active Food Packaging Coatings Based on Hybrid Electrospun Gliadin Nanofibers Containing Ferulic Acid/Hydroxypropyl-Beta-Cyclodextrin Inclusion Complexes. Nanomaterials **2018**, 8, doi:10.3390/nano8110919.
29. Celebioglu, A.; Uyar, T. Development of ferulic acid/cyclodextrin inclusion complex nanofibers for fast - dissolving drug delivery system. International Journal of Pharmaceutics **2020**, 584, doi:10.1016/j.ijpharm.2020.119395.
30. Irani, M.; Sadeghi, G.M.M.; Haririan, I. The sustained delivery of temozolomide from electrospun PCL-Diol-b-PU/gold nanocompsite nanofibers to treat glioblastoma tumors. Materials Science and Engineering C-Materials for Biological Applications **2017**, 75, 165-174, doi:10.1016/j.msec.2017.02.029.
31. Deng, L.L.; Li, Y.; Feng, F.Q.; Wu, D.; Zhang, H. Encapsulation of allopurinol by glucose cross-linked gelatin/zein nanofibers: Characterization and release behavior. Food Hydrocolloids **2019**, 94, 574-584, doi:10.1016/j.foodhyd.2019.04.004.
32. Jia, Q.Q.; Lin, X.H.; Yang, Y.W.; Duan, B. Multifunctional edible chitin nanofibers/ferulic acid composite coating for fruit preservation. Journal of Polymer Science **2023**, doi:10.1002/pol.20230054.
33. Panwar, R.; Sharma, A.K.; Kaloti, M.; Dutt, D.; Pruthi, V. Characterization and anticancer potential of ferulic acid-loaded chitosan nanoparticles against ME-180 human cervical cancer cell lines. Applied Nanoscience **2016**, 6, 803-813, doi:10.1007/s13204-015-0502-y.
34. Yang, H.; Feng, K.; Wen, P.; Zong, M.H.; Lou, W.Y.; Wu, H. Enhancing oxidative stability of encapsulated fish oil by incorporation of ferulic acid into electrospun zein mat. Lwt-Food Science and Technology **2017**, 84, 82-90, doi:10.1016/j.lwt.2017.05.045.
35. Narayanan, G.; Boy, R.; Gupta, B.S.; Tonelli, A.E. Analytical techniques for characterizing cyclodextrins and their inclusion complexes with large and small molecular weight guest molecules. Polymer Testing **2017**, 62, 402-439, doi:10.1016/j.polymertesting.2017.07.023.
36. Yu, D.G.; Li, J.J.; Williams, G.R.; Zhao, M. Electrospun amorphous solid dispersions of poorly water-soluble drugs: A review. Journal of Controlled Release **2018**, 292, 91-110, doi:10.1016/j.jconrel.2018.08.016.
37. Huang, W.D.; Yang, Y.Y.; Zhao, B.W.; Liang, G.Q.; Liu, S.W.; Liu, X.L.; Yu, D.G. Fast Dissolving of Ferulic Acid via Electrospun Ternary Amorphous Composites Produced by a Coaxial Process. Pharmaceutics **2018**, 10, doi:10.3390/pharmaceutics10030115.
38. Kumar, N.; Goel, N. Phenolic acids: Natural versatile molecules with promising therapeutic applications. Biotechnology reports (Amsterdam, Netherlands) **2019**, 24, e00370, doi:10.1016/j.btre.2019.e00370.
39. Kim, Y.J.; Park, M.R.; Kim, M.S.; Kwon, O.H. Polyphenol-loaded polycaprolactone nanofibers for effective growth inhibition of human cancer cells. Materials Chemistry and Physics **2012**, 133, 674-680, doi:10.1016/j.matchemphys.2012.01.050.
40. Yakub, G.; Ignatova, M.; Manolova, N.; Rashkov, I.; Markova, N. Chitosan/ferulic acid-coated poly(ε-caprolactone) electrospun materials with antioxidant, antibacterial and antitumor properties. International Journal of Biological Macromolecules **2018**, 107, 689-702, doi:10.1016/j.ijbiomac.2017.08.183.
41. Yu, D.G.; Yang, J.M.; Branford-White, C.; Lu, P.; Zhang, L.; Zhu, L.M. Third generation solid dispersions of ferulic acid in electrospun composite nanofibers. International Journal of Pharmaceutics **2010**, 400, 158-164, doi:10.1016/j.ijpharm.2010.08.010.
42. Kajdic, S.; Planinsek, O.; Gasperlin, M.; Kocbek, P. Electrospun nanofibers for customized drug-delivery systems. Journal of Drug Delivery Science and Technology **2019**, 51, 672-681, doi:10.1016/j.jddst.2019.03.038.
43. Kalu, V.D.; Odeniyi, M.A.; Jaiyeoba, K.T. Matrix properties of a new plant gum in controlled drug delivery. Archives of Pharmacal Research **2007**, 30, 884-889, doi:10.1007/bf02978841.

44. Ferrari, P.C.; Oliveira, G.F.; Chibebe, F.C.S.; Evangelista, R.C. In vitro characterization of coevaporates containing chitosan for colonic drug delivery. Carbohydrate Polymers **2009**, 78, 557-563, doi:10.1016/j.carbpol.2009.05.021.